

Electronic Supplementary Information

N-terminalized titanium carbide MXene coupled with graphene oxide toward optimized temporal domain-dependent nonlinear absorption

Naying Shan,^a Zihao Guan,^a Zhiyuan Wei,^a Yang Zhao,^a Fang Liu,^a Lu Chen,^a Yanyan Xue,^b Zhipeng Huang,^a Mark G. Humphrey,^c Jun Xu,^b Lulu Fu,^{a,*} and Chi Zhang^{a,*}

^a School of Chemical Science and Engineering, Tongji University, Shanghai 200092, P.R. China.

^b School of Physical Science and Engineering, Tongji University, Shanghai 200092, P.R. China.

^c Research School of Chemistry, Australian National University, Canberra, ACT 2601, Australia

Experimental section

Preparation of GO: First, graphite powder (2 g) was suspended in 45 mL of concentrated sulfuric acid (H_2SO_4 , 95 ~ 98 wt%) in a 500 mL round-bottom flask, and the mixture was stirred for 30 minutes, resulting in a dark green solution. Subsequently, 6 g of potassium permanganate (KMnO_4) was gradually introduced into the mixture in an ice bath. The stirring was sustained for 2 hours at 35 °C, leading to the formation of a brown solution. Following this, 90 mL of deionized water was added, causing the reaction temperature to rapidly rise to 95 °C. The mixture was stirred vigorously for an additional 30 minutes. Finally, 10 mL of hydrogen peroxide (H_2O_2 , 30 wt%) and 150 mL of deionized water were added to remove the residual manganese ions to obtain a bright yellow solution. Graphene oxide (GO) was isolated by centrifugation, washed with deionized water, and dried in a vacuum oven.

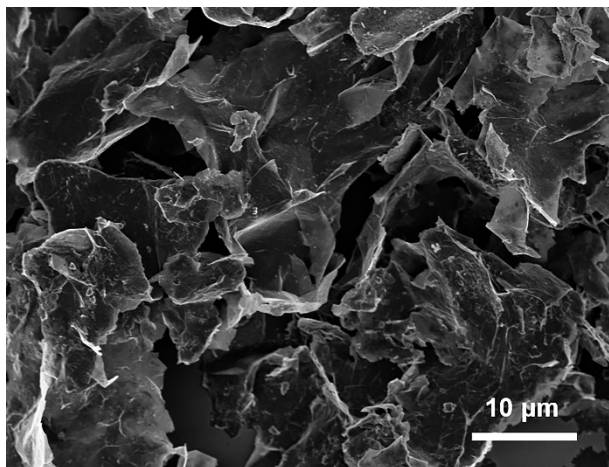


Fig. S1 The SEM image of MXene.

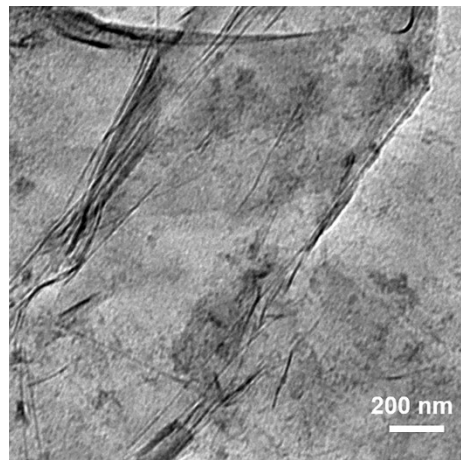


Fig. S2 The TEM image of MXene.

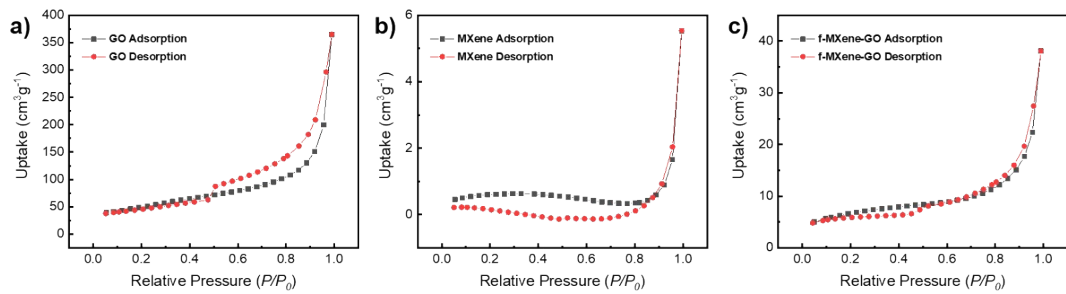


Fig. S3 N_2 adsorption-desorption isotherm of GO, MXene, and f-MXene-GO. The GO, MXene, and f-MXene-GO exhibited surface areas at 177.3 , 2.0 , and $22.9 \text{ m}^2 \text{ g}^{-1}$, respectively.

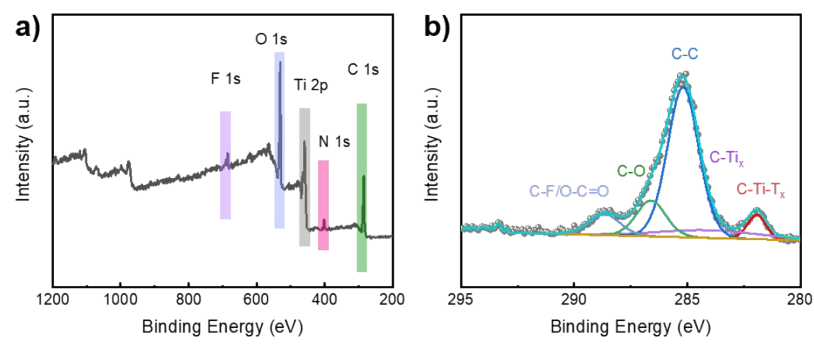


Fig. S4 (a) Survey XPS spectra of MXene/GO. (b) The high-resolution C 1s spectra of MXene/GO.

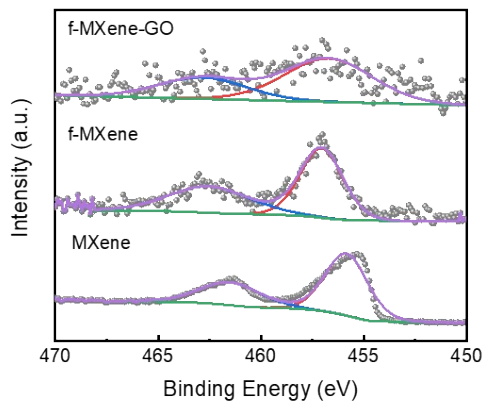


Fig. S5 Ti 2p spectra in MXene, f-MXene, and f-MXene-GO. Each peak should be subdivided into several fitting peaks, but the high-resolution Ti 2p spectra of f-MXene and f-MXene-GO were difficult to fit due to the low content.

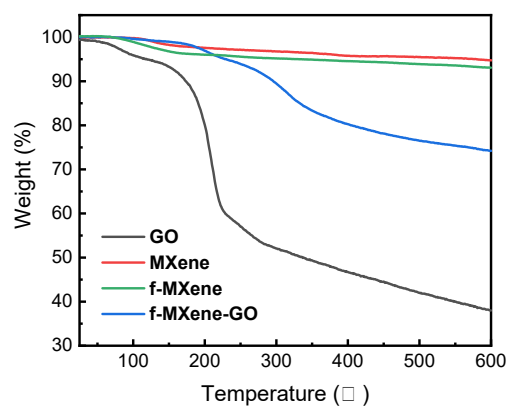


Fig. S6 TGA curve of GO, MXene, f-MXene and f-MXene-GO.

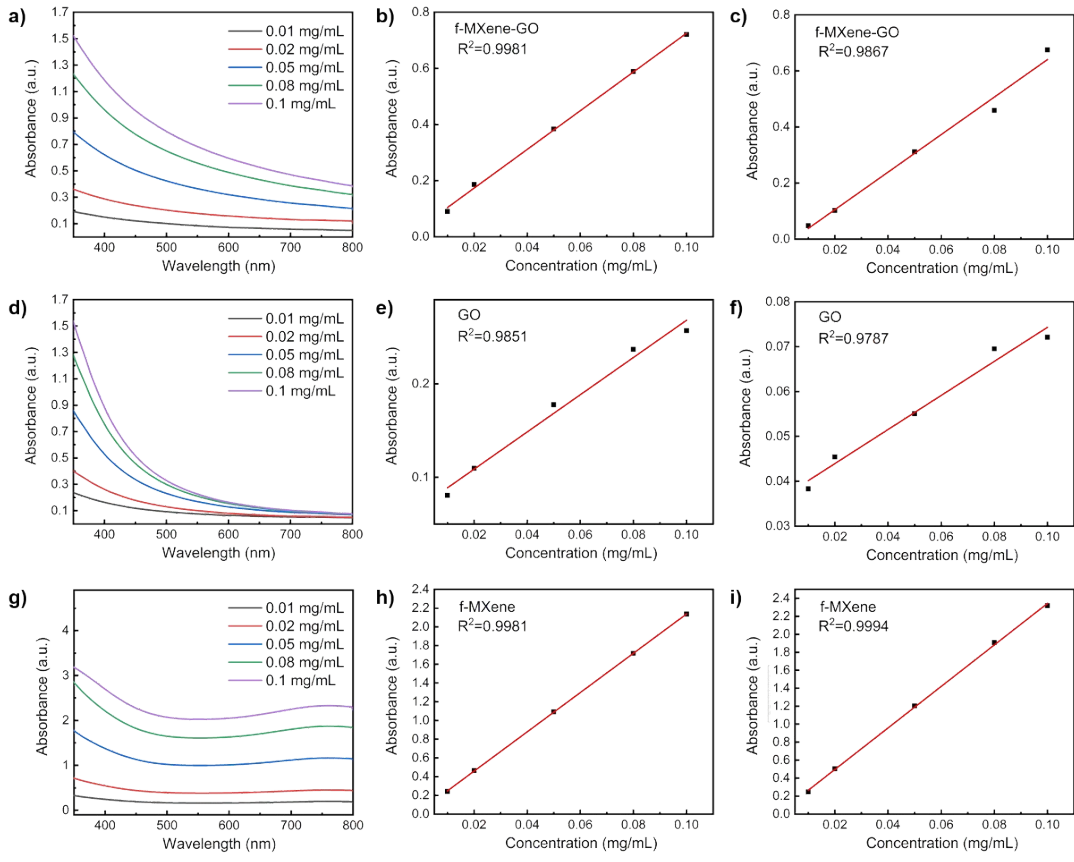


Fig. S7 The absorption spectra of (a) f-MXene-GO, (d) GO, and (g) MXene at different concentrations. The absorbance of (b) f-MXene-GO, (e) GO, and (h) MXene at different concentrations under the irradiation of 532 nm. The absorbance of (c) f-MXene-GO, (f) GO, and (i) MXene at different concentrations under the irradiation of 800 nm. The straight lines are the linear fitting results of the data.

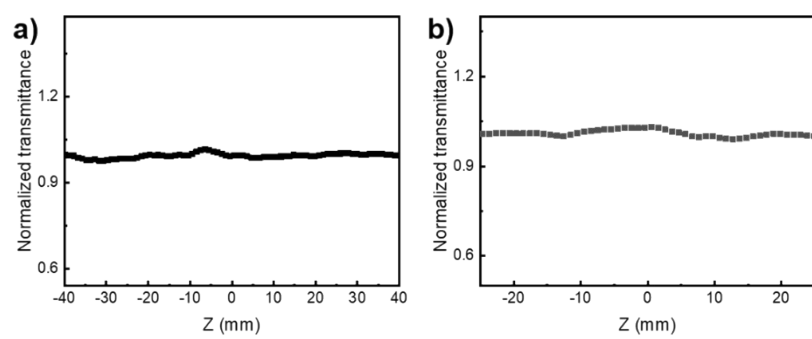


Fig. S8 Open aperture Z-scan curves for blank solvent DMF (a) in the nanosecond (ns) regime of 532 nm under input fluence energy of 125 μ J and (b) in the femtosecond (fs) regime of 800 nm under input fluence energy of 80 nJ.

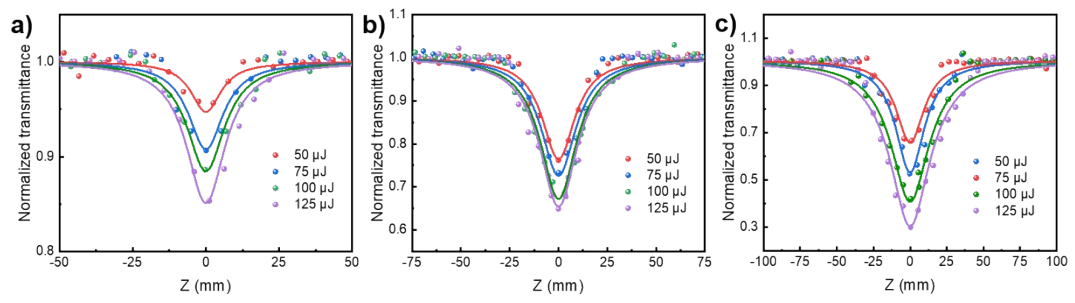


Fig. S9 Open-aperture Z-scan NLO data of (a) GO, (b) f-MXene, and (c) f-MXene-GO with the excitation of a 12 ns and 10 Hz laser centered at 532 nm.

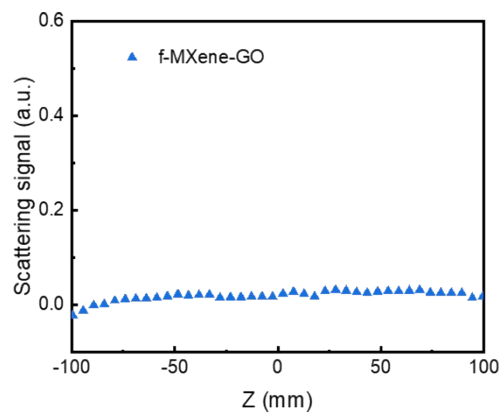


Fig. S10 Z-scan scattering results of f-MXene-GO dispersions under ns pulses with fluence energy of 125 μ J.

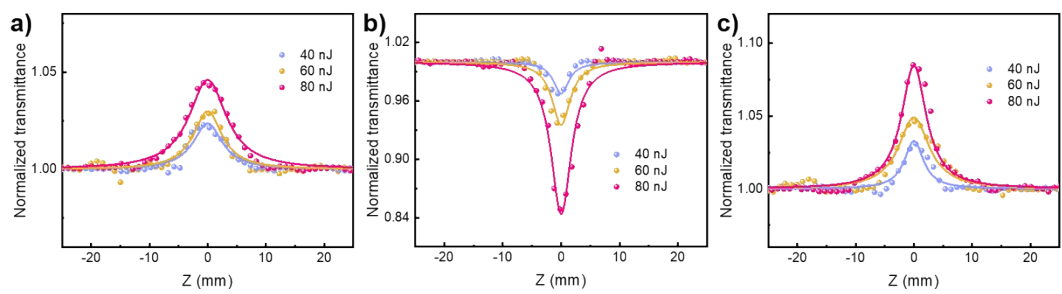


Fig. S11 Open-aperture Z-scan NLO data of (a) GO, (b) f-MXene, and (c) f-MXene-GO with the excitation of a 34 fs and 1 kHz laser centered at 800 nm.

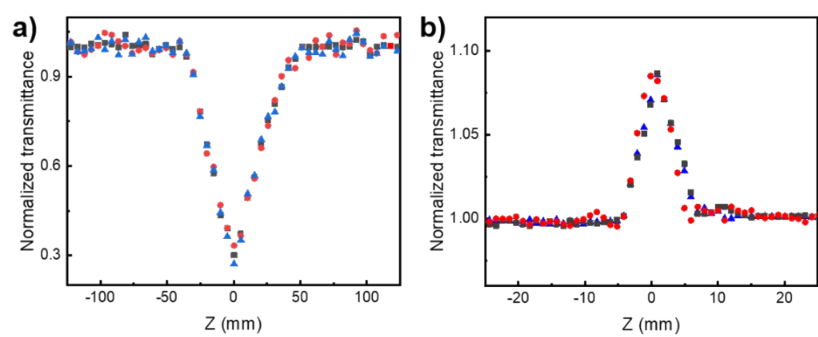


Fig. S12 (a) The open-aperture Z-scan results of f-MXene-GO in the ns regime of 532 nm at the incident pulse energies of 125 μ J for 0-day, 30-day, and 60-day storage and (b) in the fs regime of 800 nm at the incident pulse energies of 80 nJ for 0-day, 30-day, and 60-day storage.

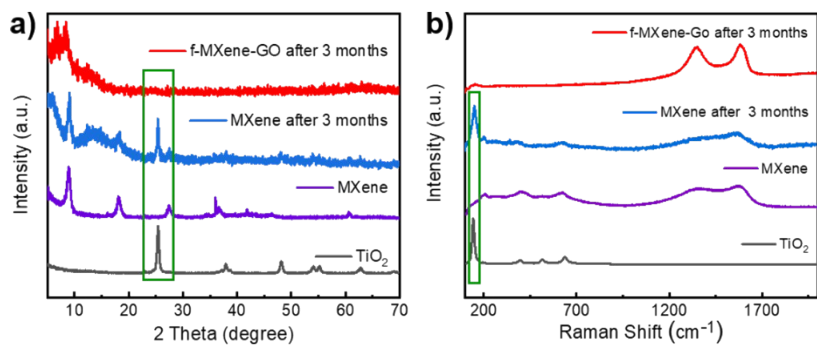


Fig. S13 (a) The XRD patterns of MXene, MXene for 3-month storage, f-MXene-GO for 3-month storage, and TiO₂. (b) The Raman spectra of MXene, MXene for 3-month storage, f-MXene-GO for 3-month storage, and TiO₂.

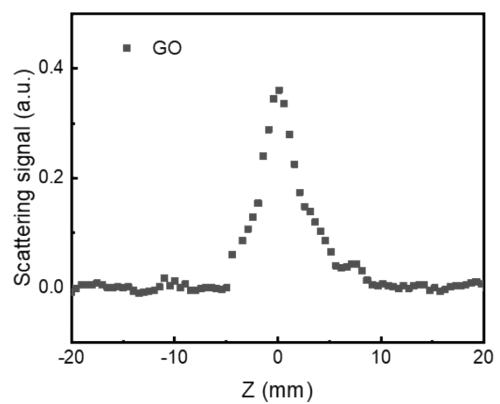


Fig. S14 Z-scan scattering results of GO dispersions under ns pulses with fluence energy of 125 μ J.

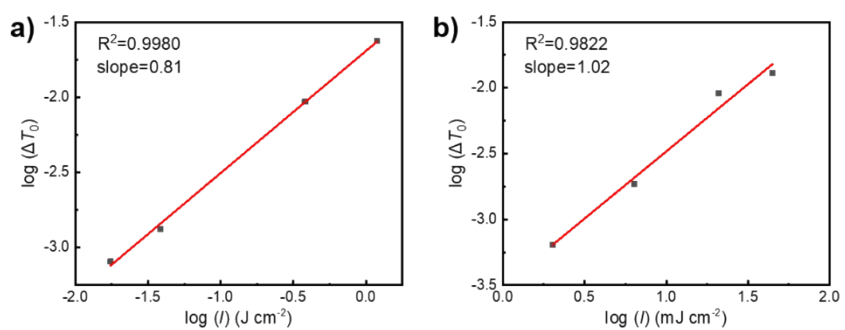


Fig. S15 Plots of $\log(\Delta T_0)$ versus $\log(I)$ for MXene (a) in the ns regime of 532 nm and (b) in the fs regime of 800 nm.

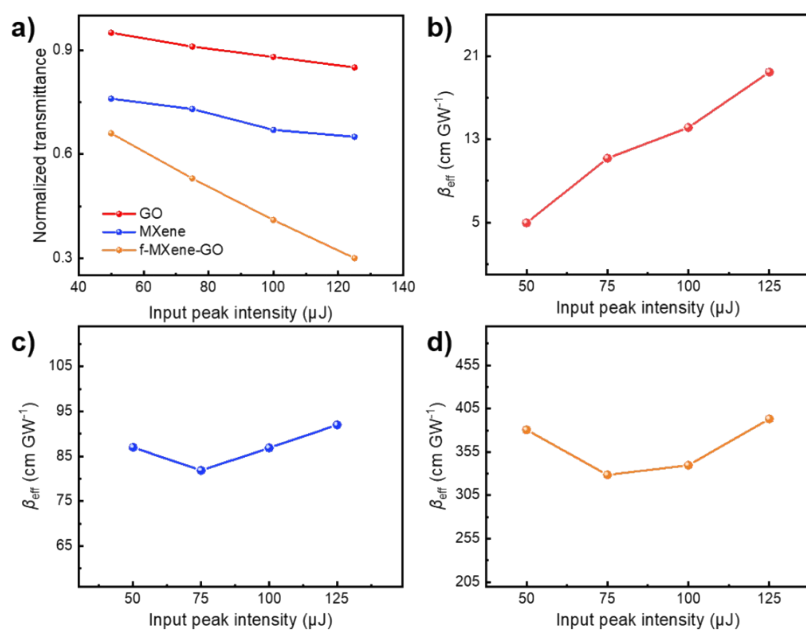


Fig. S16 (a) The plots of normalized transmittance versus input fluence in the ns regime of 532 nm. Variation of β_{eff} at ns pulses excitation with different input peak intensities for (b) GO, (c) MXene, and (d) f-MXene-GO.

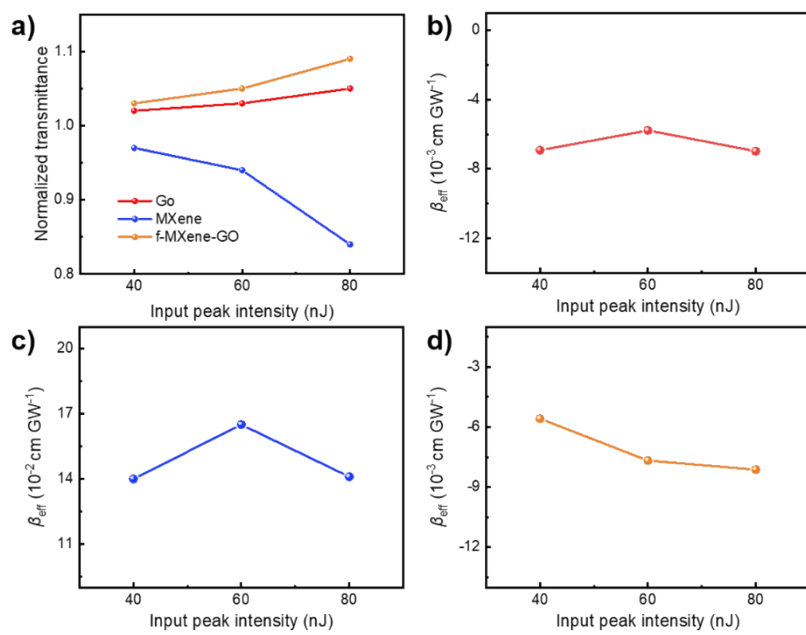


Fig. S17 (a) The plots of normalized transmittance versus input fluence in the fs regime of 800 nm. Variation of β_{eff} at fs pulses excitation with different input peak intensities for (b) GO, (c) MXene, and (d) f-MXene-GO.

Table S1 The atomic percentages in corresponding samples.

Element	Atom (%)			
	GO	MXene	f-MXene	f-MXene-GO
C 1s	74.34	47.68	44.02	62.90
O 1s	25.66	15.03	35.97	34.51
N 1s		—	3.25	1.34
F 1s	—	14.20	5.12	1.34
Ti 2p	—	23.09	11.64	0.51

Table S2 Performance comparison of RSA materials. β_{eff} : nonlinear absorption coefficient; $\text{Im}\chi^{(3)}$: third-order nonlinear susceptibility; the figure of merit (FOM) for the third-order optical nonlinearity is defined to eliminate the discrepancy caused by the linear absorption.

Materials	Laser parameters	β_{eff} (cm GW ⁻¹)	$\text{Im}\chi^{(3)}$ (esu)	FOM (esu cm ⁻¹)	Ref
TPP	532 nm,	33	—	—	1
MWCNT-TPP	11.7 ns, 10 Hz	255	—	—	
Pt NP/rGO		1.38	—	—	
Ni NP/rGO	532 nm,	1.29	—	—	2
Pt-Ni NP/rGO	4 ns, 1 Hz	1.64	—	—	
Pt-Ni NP cluster/rGO		1.98	—	—	
Mn-TMPP CPs		9	2.99×10^{-12}	—	
Zn-TMPP CPs	532 nm,	46	1.523×10^{-11}	—	3
Mn-THPP CPs	4 ns, 10 Hz	9	2.83×10^{-12}	—	
Zn-THPP CPs		18	5.92×10^{-12}	—	
Co-THPP (crystalline plates)		24	8.02×10^{-12}	—	
Co-THPP (flower-shaped clusters)	532 nm, 4 ns, 10 Hz	70	2.305×10^{-11}	—	4
Co-THPP (ultrathin films)		95	3.129×10^{-11}	—	
Copper porphyrin in DMF	532 nm,	132	—	—	5
Zinc porphyrin in DMF	6 ns, 10 Hz	366	—	—	
Ni ₃ HHTP ₂ in water	532 nm,	20	6.84×10^{-15}	—	6
Cu ₃ HHTP ₂ in water	15 ns, 10 Hz	133	4.79×10^{-14}	—	
P ₁ Pt	532 nm,	39	1.9×10^{-19}	—	7
P ₂ Pt	8 ns, 10 Hz	45	2.2×10^{-19}	—	
ZnTNP-PAES	532 nm,	5.28	—	—	8
ZnP-GO	6 ns, 10 Hz	2.80	—	—	
PF-GO		4.99	—	—	
ZnP-RGO	532 nm, 6 ns, 10 Hz	6.58	—	—	8
PF-RGO		7.07	—	—	
BP/PMMA	532 nm,	8.43	3.60×10^{-12}	—	9
	6 ns, 2 Hz				

F ₁₆ PcGaCl/PMMA		74.92	3.199 × 10 ⁻¹¹	—	
F ₁₆ PcGa-BP/PMMA		282.86	1.21 × 10 ⁻¹⁰	—	
rGO/PMMA		129.01	5.509 × 10 ⁻¹¹	—	
PFTP-rGO/PMMA	532 nm, 6 ns, 2 Hz	215.77	9.213 × 10 ⁻¹¹	—	¹⁰
annealed PFTP-rGO/PMMA		296.79	1.267 × 10 ⁻¹⁰	—	
BP:C ₆₀ /PMMA	532 nm, 6 ns, 2 Hz	39.39	1.682 × 10 ⁻¹¹	1.47 × 10 ⁻¹³	
annealed BP:C ₆₀ /PMMA		241.73	1.03 × 10 ⁻¹⁰	1.70 × 10 ⁻¹²	¹¹
annealed BP:C ₆₀ solvent		4.62	1.59 × 10 ⁻¹⁵	3.70 × 10 ⁻¹³	
C ₆₀ -MXene	532 nm,	74.9	2.63 × 10 ⁻¹¹	—	¹²
C ₇₀ -MXene	12 ns, 10 Hz	70.0	2.46 × 10 ⁻¹¹	—	
Au ₃₈	532 nm,	35	—	—	¹³
Au ₁₄₄	5 ns	75	—	—	
f-MXene-GO	532 nm, 12 ns, 10 Hz	393.13	1.34 × 10 ⁻¹⁰	7.72 × 10 ⁻¹¹	this work

Table S3 Performance comparison of optical limiting threshold (F_{OL}).

Samples	Laser parameters	F_{OL} (J cm $^{-2}$)	Ref.
PIZA-1 film	532 nm, 5 ns, 10 Hz	5.51	14
C ₆₀ @PIZA-1 film		5.04	
Copper porphyrin in DMF	532 nm, 6 ns, 10 Hz	1.7	5
Zinc porphyrin in DMF		1.3	
Ni ₃ HHTP ₂ in water		4.19	
Cu ₃ HHTP ₂ in water	532 nm, 15 ns, 10 Hz	1.83	6
Co ₃ HHTP ₂ in water		3.03	
Pt-Ni NP/rGO	532 nm, 4 ns, 1 Hz	2.39	2
Pt-Ni NP cluster/rGO		1.42	
F ₁₆ PcGa-BP/PMMA	532 nm, 6 ns, 2 Hz	2.64	9
F ₁₆ PcGaCl/PMMA		9.24	
TPC	532 nm, 7 ns, 10 Hz	1.04	15
C ₆₀		12.85	
Trithiasumanene	532 nm, 8 ns, 10 Hz	2.43	16
Pyrazine-fused triselenasumanene		1.78	
CTS@CuBDC film	532 nm, 5 ns, 10 Hz	0.92	17
Sa-TAPA COF in acetone	532 nm, 6 ns, 10 Hz	2.38	18
PTC-271/KBr	532 nm, 5 ns, 5 Hz	4.42	19
PTC-272/KBr		0.669	
MoS ₂ in NMP		11.16	
MoSe ₂ in NMP		7.3	
WS ₂ in NMP	532 nm, 6 ns, 2 Hz	9.35	20
WSe ₂ in NMP		7.2	
Graphene in NMP		15.15	
f-MXene-GO	532 nm, 12 ns, 10 Hz	0.49	this work

Table S4 Linear and NLO parameters of GO, MXene, MXene/GO, and f-MXene-GO in the ns regime of 532 nm (125 μ J) and the fs regime of 800 nm (80 nJ). α_0 : linear absorption coefficient; β_{eff} : nonlinear absorption coefficient; $\text{Im}\chi^{(3)}$: third-order nonlinear susceptibility; the figure of merit (FOM) for the third-order optical nonlinearity is defined to eliminate the discrepancy caused by the linear absorption.

Samples	Laser	α_0 (cm $^{-1}$)	β_{eff} (cm GW $^{-1}$)	$\text{Im}\chi^{(3)}$ (esu)	FOM (esu cm $^{-1}$)
GO	532 nm	1.20	19.47	6.65×10^{-12}	5.55×10^{-12}
MXene	12 ns	5.11	92.00	3.14×10^{-11}	6.15×10^{-12}
MXene/GO	10 Hz	5.45	56.77	1.94×10^{-11}	3.56×10^{-12}
f-MXene-GO		1.74	393.13	1.34×10^{-10}	7.72×10^{-11}
GO	800 nm	0.30	-6.98×10^{-3}	-3.59×10^{-15}	1.20×10^{-14}
MXene	34 fs	5.80	1.41×10^{-2}	7.25×10^{-15}	1.25×10^{-15}
MXene/GO	1 kHz	4.78	7.03×10^{-3}	3.61×10^{-15}	7.56×10^{-16}
f-MXene-GO		0.46	-8.12×10^{-3}	-4.17×10^{-15}	9.07×10^{-15}

Table S5 Performance comparison of SA materials. I_s : saturation intensity; β_{eff} : nonlinear absorption coefficient; $\text{Im}\chi^{(3)}$: third-order nonlinear susceptibility; the figure of merit (FOM) for the third-order optical nonlinearity is defined to eliminate the discrepancy caused by the linear absorption.

Materials	Laser parameters	I_s (GW cm ⁻²)	β_{eff} (cm GW ⁻¹)	$\text{Im}\chi^{(3)}$ (esu)	FOM (esu cm ⁻¹)	Ref.
MoSe ₂ in CHP	800 nm,	590	-2.54×10^{-3}	-1.45×10^{-15}	6.9×10^{-16}	21
MoTe ₂ in CHP	100 fs, 1 kHz	217	-3.7×10^{-3}	-2.13×10^{-15}	1.45×10^{-15}	
MoS ₂ in NMP	800 nm,	413	-4.60×10^{-3}	-2.52×10^{-15}	1.06×10^{-15}	
MoS ₂ in NVP	100 fs, 1 kHz	833	-1.78×10^{-3}	-1.03×10^{-15}	6.2×10^{-16}	22
MoS ₂ in CHP		405	-5.80×10^{-3}	-3.30×10^{-15}	1.16×10^{-15}	
BP in IPA	800 nm,	334.6	-6.17×10^{-3}	—	—	
BP in NMP	100 fs, 1 kHz	647.7	-4.08×10^{-3}	—	—	23
BP in EA		261.3	-2.87×10^{-3}	—	—	
MWNTs-TPP/PMMA	800 nm, 130 fs, 1 kHz	—	-3.6×10^{-3}	—	—	24
Graphene in DMF		23	—	—	5.0×10^{-15}	
Graphene in THF	790 nm,	26	—	—	3.3×10^{-15}	25
Graphene in H ₂ O	50 fs, 1 kHz	25	—	—	3.6×10^{-15}	
GO		8	—	—	4.2×10^{-15}	
rGO	790 nm,	170	—	—	3.6×10^{-16}	26
BCN	80 fs, 1 kHz	—	—	—	2.4×10^{-15}	
AgInSe ₂ nanorods	780 nm, 200 fs, 1 kHz	—	—	—	8×10^{-15}	27
Au nanorods	780 nm, 220 fs, 1 kHz	—	—	—	8.8×10^{-16}	28
f-MXene-GO	800 nm, 34 fs, 1 kHz	62.72	-8.12×10^{-3}	-4.17×10^{-15}	9.07×10^{-15}	this work

Calculation of Nonlinear Absorption Parameters

The total absorption coefficient of the material can be written as

$$\alpha(I) = -\alpha_0 + \beta I \quad (\text{Equation S1})$$

where α_0 and β are linear absorption coefficients and nonlinear absorption coefficients, respectively. I is the incident light intensity.

The corresponding light propagation model is expressed as²⁹

$$\frac{dI}{dz} = -(\alpha_0 + \beta I)I \quad (\text{Equation S2})$$

As for open aperture Z-scan, the normalized transmittance can be given as²⁹

$$T(z) = \sum_{m=0}^{\infty} \frac{\left[\frac{-\beta_{eff} I_0 L_{eff}}{1 + \frac{Z^2}{Z_0^2}} \right]_m}{(m+1)^{\frac{3}{2}}} \quad (\text{Equation S3})$$

$$L_{eff} = \frac{(1 - e^{-\alpha_0 L})}{\alpha_0} \quad (\text{Equation S4})$$

where L_{eff} is the effective interaction length, α_0 is the linear absorption coefficient, L is the sample thickness, β_{eff} is the nonlinear absorption coefficient, I_0 is the on-axis peak intensity at the focal plane, and z_0 is the Rayleigh diffraction length. By fitting the experimental data, the nonlinear absorption coefficient β_{eff} can be obtained.

The imaginary part of the third-order nonlinear susceptibility ($Im\chi^{(3)}$) was calculated according to

$$Im\chi^{(3)} = \left[\frac{10^{-7} c \lambda n^2}{96\pi^2} \right] \beta_{eff} \quad (\text{Equation S5})$$

where c is the speed of light, λ is the wavelength of the laser, and n is the refractive index.

The figure of merit (FOM) for the third-order optical nonlinearity is defined as

$$FOM = |\text{Im}\chi^{(3)} / \alpha_0|$$

After transforming the normalized transmittance as a function of laser intensity, we can obtain the saturation intensity (I_s) by fitting the curves with a nonlinear transmission model.³⁰⁻³² I_s describing the saturable photoinduced electron-hole density is the degree of difficulty of being fully saturated and the most important parameter to consider for saturable absorption.

$$T(I) = A * \exp\left(\frac{-\Delta T}{1 + I/I_s}\right)$$

Where $T(I)$ is the intensity-dependent transmission, ΔT , I_s , and A are modulation depth, saturation intensity, and normalization constant, respectively.

Theoretical Calculation Methods

All the computational simulations in this work were performed by using spin-polarized density functional theory (DFT) calculations. The Cambridge Serial Total Energy Package (CASTEP) module implemented in Material Studio software was used.^{33,34} The exchange-correlation energy was described by using the Perdew-Burke-Ernzerhof (PBE) functional within the generalized gradient approximation (GGA), and the van der Waals dispersive interaction was described by Grimme's DFT-D2 method.^{35,36} A plane-wave cutoff energy of 400 eV was chosen in all calculations. The convergence criteria for the geometry optimization process concerning the energy, the maximum atomic force, and the maximum displacement were 1.0×10^{-5} eV, 0.03 eV Å⁻¹, and 0.001 Å, respectively. The Brillouin zone was sampled via $2 \times 2 \times 1$ k-point grids.

References

- 1 Z. Liu, Z. Guo, X. Zhang, J. Zheng and J. Tian, *Carbon*, 2013, **51**, 419-426.
- 2 C. Zheng, L. Lei, J. Huang, W. Chen, W. Li, H. Wang, L. Huang and D. Huang, *J. Mater. Chem. C*, 2017, **5**, 11579-11589.
- 3 B. W. Xu, R. J. Niu, Q. Liu, J. Y. Yang, W. H. Zhang and D. J. Young, *Dalton Trans*, 2020, **49**, 12622-12631.
- 4 R. J. Niu, W. F. Zhou, Y. Liu, J. Y. Yang, W. H. Zhang, J. P. Lang and D. J. Young, *Chem. Commun.*, 2019, **55**, 4873-4876.
- 5 M. B. M. Krishna, V. P. Kumar, N. Venkatramaiyah, R. Venkatesan and D. N. Rao, *Appl. Phys. Lett.*, 2011, **98**, 081106.
- 6 Y. Sun, H. Li, X. Gao, Z. Yu, Z. Huang and C. Zhang, *Adv. Opt. Mater.*, 2021, **9**, 2100622.
- 7 Z. Liu, J. Sun, C. Yan, Z. Xie, G. Zhang, X. Shao, D. Zhang and S. Zhou, *J. Mater. Chem. C*, 2020, **8**, 12993-13000.
- 8 Y. Du, N. Dong, M. Zhang, K. Zhu, R. Na, S. Zhang, N. Sun, G. Wang and J. Wang, *Phys. Chem. Chem. Phys.*, 2017, **19**, 2252-2260.
- 9 Z. Liu, B. Zhang, N. Dong, J. Wang and Y. Chen, *J. Mater. Chem. C*, 2020, **8**, 10197-10203.
- 10 Z. Liu, N. Dong, P. Jiang, K. Wang, J. Wang and Y. Chen, *Chemistry-a European Journal*, 2018, **24**, 19317-19322.
- 11 M. Shi, S. Huang, N. Dong, Z. Liu, F. Gan, J. Wang and Y. Chen, *Chem. Commun.*, 2018, **54**, 366-369.
- 12 Y. Fang, Z. Wei, Z. Guan, N. Shan, Y. Zhao, F. Liu, L. Fu, Z. Huang, M. G. Humphrey and C. Zhang, *J. Mater. Chem. C*, 2023, **11**, 7331-7344.
- 13 K. Wang, J. Zhou, L. Yuan, Y. Tao, J. Chen, P. Lu and Z. L. Wang, *Nano Lett.*, 2012, **12**, 833-838.
- 14 D. Li, Z. Gu and J. Zhang, *Chem. Sci.*, 2020, **11**, 1935-1942.
- 15 M. V. Vijisha, J. Ramesh, C. Arunkumar and K. Chandrasekharan, *J. Mater. Chem. C*, 2020, **8**, 12689-12697.
- 16 J. Sun, Y. Sun, C. Yan, D. Lin, Z. Xie, S. Zhou, C. Yuan, H.-L. Zhang and X.

- Shao, *J. Mater. Chem. C*, 2018, **6**, 13114-13119.
- 17 Y. Zhu, Y. Kang, Z. Gu and J. Zhang, *Adv. Opt. Mater.*, 2021, **9**, 2002072.
- 18 X. Li, Q. Gao, J. Aneesh, H.-S. Xu, Z. Chen, W. Tang, C. Liu, X. Shi, K. V. Adarsh, Y. Lu and K. P. Loh, *Chem. Mater.*, 2018, **30**, 5743-5749.
- 19 M.-Y. Gao, Z. Wang, Q.-H. Li, D. Li, Y. Sun, Y. H. Andaloussi, C. Ma, C. Deng, J. Zhang and L. Zhang, *J. Am. Chem. Soc.*, 2022, **144**, 8153-8161.
- 20 N. Dong, Y. Li, Y. Feng, S. Zhang, X. Zhang, C. Chang, J. Fan, L. Zhang and J. Wang, *Sci. Rep.*, 2015, **5**, 14646.
- 21 K. Wang, Y. Feng, C. Chang, J. Zhan, C. Wang, Q. Zhao, J. N. Coleman, L. Zhang, W. J. Blau and J. Wang, *Nanoscale*, 2014, **6**, 10530-10535.
- 22 K. Wang, J. Wang, J. Fan, M. Lotya, A. O'Neill, D. Fox, Y. Feng, X. Zhang, B. Jiang, Q. Zhao, H. Zhang, J. N. Coleman, L. Zhang and W. J. Blau, *ACS Nano*, 2013, **7**, 9260-9267.
- 23 S. B. Lu, L. L. Miao, Z. N. Guo, X. Qi, C. J. Zhao, H. Zhang, S. C. Wen, D. Y. Tang and D. Y. Fan, *Opt. Express*, 2015, **23**, 11183-11194.
- 24 X.-L. Zhang, Z.-B. Liu, X. Zhao, X.-Q. Yan, X.-C. Li and J.-G. Tian, *Opt. Express*, 2013, **21**, 25277-25284.
- 25 S. Kumar, M. Anija, N. Kamaraju, K. S. Vasu, K. S. Subrahmanyam, A. K. Sood and C. N. R. Rao, *Appl. Phys. Lett.*, 2009, **95**.
- 26 S. Kumar, N. Kamaraju, K. S. Vasu, A. Nag, A. K. Sood and C. N. R. Rao, *Chem. Phys. Lett.*, 2010, **499**, 152-157.
- 27 H. I. Elim, W. Ji, M.-T. Ng and J. J. Vittal, *Appl. Phys. Lett.*, 2007, **90**.
- 28 H. I. Elim, J. Yang, J.-Y. Lee, J. Mi and W. Ji, *Appl. Phys. Lett.*, 2006, **88**.
- 29 M. Sheik-Bahae, A. A. Said, T. H. Wei, D. J. Hagan and E. W. V. Stryland, *IEEE J. Quantum Elect.*, 1990, **26**, 760-769.
- 30 X. Ma, C. Wang, J. Zhang, T. Wang, A. Wang, S. Wang, Z. Jia, B. Zhang, J. He, S. van Smaalen and X. Tao, *Adv. Opt. Mater.*, 2022, **10**, 2201087.
- 31 S. Wang, H. Yu, H. Zhang, A. Wang, M. Zhao, Y. Chen, L. Mei and J. Wang, *Adv. Mater.*, 2014, **26**, 3538-3544.
- 32 H. Yu, H. Zhang, Y. Wang, C. Zhao, B. Wang, S. Wen, H. Zhang and J. Wang,

Laser Photonics Rev., 2013, **7**, L69-L97.

- 33 M. D. Segall, J. D. L. Philip, M. J. Probert, C. J. Pickard, P. J. Hasnip, S. J. Clark
and M. C. Payne, *J. Phys.: Condens. Matter*, 2002, **14**, 2717.
- 34 D. Vanderbilt, *Phys. Rev. B*, 1990, **41**, 7892-7895.
- 35 J. P. Perdew, K. Burke and M. Ernzerhof, *Phys. Rev. Lett.*, 1996, **77**, 3865-3868.
- 36 S. Grimme, *J. Comput. Chem.*, 2006, **27**, 1787-1799.